Friction performance and optimisation of diamond-like texture on hydraulic cylinder surface

Xiaolan Chen[1,2], *Liangcai Zeng*[1,3] ✉, *Feilong Zheng*[1]

[1]*Key Laboratory of Metallurgical Equipment and Control of Ministry of Education, Wuhan University of Science and Technology, Hubei Wuhan 430081, People's Republic of China*
[2]*School of Mechanical and Electrical Engineering, Huanggang Normal University, Hubei Huanggang 438000, People's Republic of China*
[3]*Hubei Key Laboratory of Mechanical Transmission and Manufacturing Engineering, Wuhan University of Science and Technology, Hubei Wuhan 430081, People's Republic of China*
✉ *E-mail: cxl110798@126.com*

Published in Micro & Nano Letters; Received on 15th January 2018; Revised on 4th April 2018; Accepted on 6th April 2018

For the ring surface of a hydraulic cylinder, grid and striped textures have been demonstrated in many previous works to easily provide a conductive oil path, which increases the difficulty of generating converging wedges and are harmful to the formation of dynamic pressure lubrication, especially for full lubrication. Moreover, these studies used an orthogonal design method to study the hydrodynamic lubrication effect and friction performance of the surface without considering the comprehensive effect of multiple parameters with simultaneous changes, which may introduce errors into the simulation analysis. In this work, a diamond-like, non-conductive texture, which mimics shark skin, is developed and optimised to determine the optimal texture morphology while simultaneously considering the influence of multiple parameters, including the diamond angle, axial length ratio, and area occupancy, to optimise the surface of the friction pair. The results show that under the same working conditions, the lift of the diamond texture is nine times greater than that of the striped texture, while its friction coefficient is only one-quarter of that of the striped texture, which will greatly improve the friction and responsiveness of the hydraulic cylinder.

1. Introduction: Surface texturing that imitates biological surface geometries has emerged as an effective technique for improving the performance of many vital tribological components, such as piston rings [1, 2], bearings [3, 4], cutting tools [5, 6], and mechanical seals [7, 8]. Hydraulic transmission is one of the main transmission forms in the field of mechanical engineering. The low-frequency response of a hydraulic cylinder severely limits the hydraulic system, mainly due to friction between the cylinder and the piston [9]. In recent years, the development of microtexture lubrication technology has provided a new way of thinking to solve this problem.

Sharks travel rapidly by virtue of their skin surface, which is covered with diamond-like shield scales that reduce friction resistance while swimming [10]. Lu and co-workers [11] investigated the effect of a grid texture on the lubrication performance of a microcirculation surface and indicated that the grid texture on the sliding surface decreased the friction coefficient (Fig. 1*a*). A bionic striped texture was developed by Yu and his group on the piston surface of a clearance seal hydraulic cylinder, and the results showed that microstripes improve the lubrication performance on piston surfaces [12] (Fig. 1*b*).

For textured surfaces, microtextures can be regarded as converging microwedges; thus, a plurality of textures could act as a set of microbearings [13] (see Fig. 2). The figure clearly shows that besides the converging wedges at the trailing edge of the pockets, diverging wedges also appear. A positive net increase is only possible due to the presence of the texture if the increase in the pressure at the trailing edge is higher than the decrease in the pressure at the back edge of the pocket. These conditions can be satisfied by the occurrence of cavitation. For the ring surface of the hydraulic cylinder, the grid and striped textures in [11, 12] easily formed a conductive oil path, which is difficult to generate with converging wedges and prevents the formation of dynamic pressure lubrication, especially for full lubrication. Thus, the morphology of the bionic texture and its parameters greatly affects the performance of the friction pair surface.

Moreover, the influences of simultaneous changes in single and multiple parameters on the textured surface are completely different. The above-mentioned reports used an orthogonal design method to study the hydrodynamic lubrication effect and friction performance of the surface, without considering the comprehensive effects of multiple parameters with simultaneous changes, which may introduce some errors into the simulation analysis.

Here, a diamond-like texture that mimics shark skin and is non-conductive is developed and optimised to determine the optimal texture morphology while simultaneously considering the influence of multiple parameters, including the diamond angle, axial length ratio, and area occupancy, to optimise the surface of the friction pair.

2. Texturing cylinder: Since the gap between the cylinder and the piston is typically a few micrometres and is much smaller than the curvature radius of the cylinder, the influence of the gap can be ignored, and the cylinder can be unrolled into a plane for analysis [14]. The diamond-like texture imitating shark skin is applied to the cylinder wall (Fig. 3).

To simplify the calculation, a square control unit is analysed in this Letter. Suppose the sides of the square are L_x and L_y ($L_x = L_y$). The diagonal lengths of the diamond along the x and y directions are $2a$ and $2b$, respectively. Meanwhile, the texture depth is h_p (see Fig. 4).

3. Numerical model and analysis

3.1. Governing equation: The hydrodynamic pressures are calculated by solving the Reynolds equation derived from the Navier–Stokes equation by assuming the classical hypotheses of lubrication theory in [12, 14, 15]; i.e. (i) the surfaces are smooth; (ii) the film thickness is smaller than the size of the other features

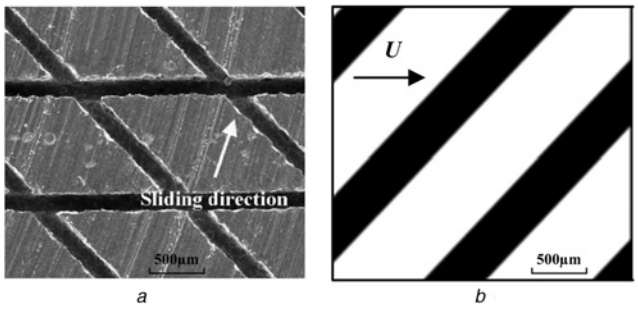

Fig. 1 *Texture*
a Grid texture and
b Stripe texture

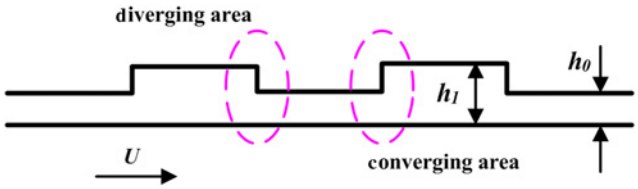

Fig. 2 *Texture effect of micro converging microwedges*

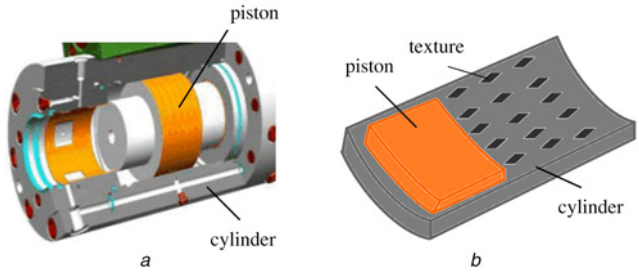

Fig. 3 *Texture configuration:*
a Friction pair and
b Shape and distribution

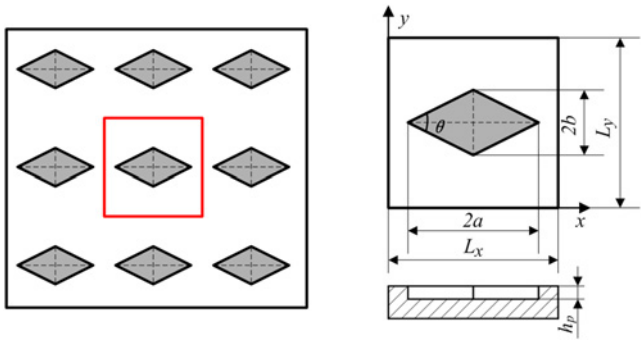

Fig. 4 *Control volume on the hydraulic cylinder surface*

at the contact interface; and (iii) the hydraulic components are rigid bodies, and the piston is not eccentric. For an isothermal and incompressible lubricant, the Reynolds equation can be written as

$$\frac{\partial}{\partial x}\left(\rho h^3 \frac{\partial p}{\partial x}\right) + \frac{\partial}{\partial y}\left(\rho h^3 \frac{\partial p}{\partial y}\right) = 6\eta \frac{\partial}{\partial x}(U\rho h), \tag{1}$$

where p is the hydrodynamic pressure, η is the oil dynamic viscosity, U is the sliding velocity of the piston, ρ is the density of oil, and h is the film thickness.

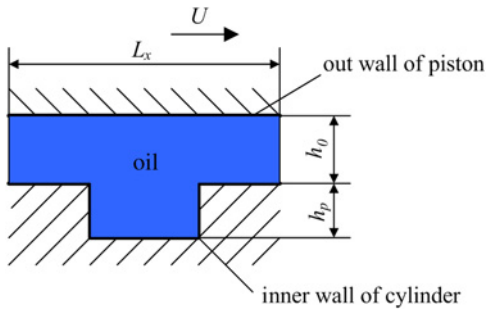

Fig. 5 *Film thickness between the piston and cylinder*

3.2. Film thickness equation: Considering the cylinder surface as the coordinate plane, and then the film thickness equation can be expressed as (Fig. 5)

$$h(x, y) = \begin{cases} h_0 & (x, y) \notin \Omega, \\ h_0 + h_p & (x, y) \in \Omega, \end{cases} \tag{2}$$

where Ω is the diamond-like region and can be given by

$$|b|\left(x - \frac{L_x}{2}\right) + |a|\left(y - \frac{L_y}{2}\right) = |ab|. \tag{3}$$

The terms a, b are the half of the diamond diagonal, respectively. Then diamond angle (defined as θ), axial length ratio (defined as γ), and area occupancy (defined as s_p) can be expressed as

$$\theta = 2\arctan\frac{b}{a}, \quad \gamma = \frac{b}{a}, \quad s_p = 2ab, \tag{4}$$

3.3. Boundary conditions: The Reynolds cavitation boundary is described as the starting point of the oil film rupture, which must be equal to zero, and the oil film pressure and gradient of the normal pressure in the cavitation area must be simultaneously zero. Therefore, it can be expressed as

$$\begin{cases} p(0, y) = p(L_x, y) = p(x, 0) = p(x, L_y) = p_0, \\ \left(\dfrac{\partial p}{\partial h}\right)_{p=p_{\text{cav}}} = 0, \end{cases} \tag{5}$$

where p_0 is the standard atmospheric pressure and p_{cav} is the saturated vapour pressure of the hydraulic oil.

4. Numerical calculations and simulation

4.1. Calculation of friction parameters: According to Wen [15], the hydrodynamic lift (also known as the bearing capacity) can be obtained by integrating the pressure along the lubrication area since the forces acting on the microelements are equal in all directions. Therefore, after calculating the pressure distribution of the oil film with (1), the friction parameters can be solved.

Over the entire range of the lubricating film, the pressure can be integrated to obtain the bearing capacity of the lubricating film (defined as W) as

$$W = \int_0^{L_y}\int_0^{L_x} p\mathrm{d}x\mathrm{d}y. \tag{6}$$

Meanwhile, the friction force exerted by the lubricating film (defined as F) on the solid surface can be obtained by integrating the shear stress in the fluid layer, which is in contact with the

doi: 10.1049/mnl.2018.0026

surface over the entire lubricating film

$$F = \int_0^{L_y} \int_0^{L_x} \left(\frac{h}{2} \frac{\partial p}{\partial x} + U \frac{\eta}{h} \right) \mathrm{d}x\mathrm{d}y. \tag{7}$$

Finally, the friction coefficient (defined as μ) on the hydraulic cylinder surface can be obtained

$$\mu = \frac{F}{W}. \tag{8}$$

4.2. Calculation method: The Reynolds equation is an elliptic second-order partial differential equation, which is difficult to solve analytical solution with the existing mathematical theory. Most discretisation methods are applicable for this kind of equation and many have been successfully applied in the field of surface texturing (e.g. finite difference method (FDM) [16], finite volume method [17], finite element method [18], finite cell method [19] and spectral element method) [18]. Due to the ease of implementation, FDM is the most popular discretisation method used in the study of textured surfaces. Therefore, the FDM is used to solve (1) in this Letter.

To universalise the solutions, the parameters in (1) and (2) should be non-dimensional

$$X = \frac{x}{L_x}, \quad Y = \frac{y}{L_y}, \quad H = \frac{h}{h_0}, \quad P = \frac{p}{p_0}. \tag{9}$$

Then, (1) and (2) can be simplified as

$$\frac{\partial}{\partial X}\left(H^3 \frac{\partial P}{\partial X} \right) + \frac{\partial}{\partial Y}\left(H^3 \frac{\partial P}{\partial Y} \right) = \left(\frac{6U\eta L_x}{h_0 p_0} \right) \frac{\partial H}{\partial X}, \tag{10}$$

$$H = \begin{cases} 1 & (X, Y) \notin \Omega, \\ 1 + \dfrac{h_p}{h_0} & (X, Y) \in \Omega. \end{cases} \tag{11}$$

The five-point difference method is used to solve (10). The parameters X and Y are divided into M and N grids in the interval [0, 1], respectively (Fig. 6). The total numbers of nodes will be equal to $M+1$.

Then $P(i,j)$ of every node can be calculated using the other four surrounding nodes

$$\begin{cases} \dfrac{\partial}{\partial X}\left(H^3 \dfrac{\partial P}{\partial X} \right) = \dfrac{H_{i+1,j}^3 P_{i+1,j} + H_{i,j}^3 P_{i-1,j} - \left(H_{i+1,j}^3 + H_{i,j}^3 \right) P_{i,j}}{\Delta X^2}, \\ \dfrac{\partial}{\partial Y}\left(H^3 \dfrac{\partial P}{\partial Y} \right) = \dfrac{H_{i,j+1}^3 P_{i,j+1} + H_{i,j}^3 P_{i,j-1} - \left(H_{i,j+1}^3 + H_{i,j}^3 \right) P_{i,j}}{\Delta Y^2}, \\ \dfrac{\partial H}{\partial X} = \dfrac{H_{i+1,j} - H_{i,j}}{\Delta X}. \end{cases} \tag{12}$$

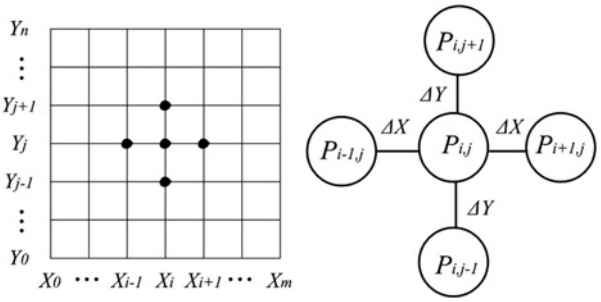

Fig. 6 *Five-point difference method*

Thus, (10) can be simplified as

$$P(i,j) = AP_{i+1,j} + BP_{i-1,j} + CP_{i,j+1} + DP_{i,j-1} + E, \tag{13}$$

where the terms A, B, C, D, and E can be given as

$$\begin{aligned} A &= \frac{\Delta Y^2 H^3 i+1, j}{\left(\Delta X^2 + \Delta Y^2\right)\left(H^3 i+1, j + H^3 i, j\right)}, \\ B &= \frac{\Delta Y^2 H^3 i, j}{\left(\Delta X^2 + \Delta Y^2\right)\left(H^3 i+1, j + H^3 i, j\right)}, \\ C &= \frac{\Delta X^2 H^3 i, j+1,}{\left(\Delta X^2 + \Delta Y^2\right)\left(H^3 i+1, j + H^3 i, j\right)}, \\ D &= \frac{\Delta X^2 H^3 i, j-1}{\left(\Delta X^2 + \Delta Y^2\right)\left(H^3 i+1, j + H^3 i, j\right)}, \\ E &= \frac{6U\eta L_x \Delta X \Delta Y^2 H^3 i+1, j}{h_0^2 p_0 \left(\Delta X^2 + \Delta Y^2\right)\left(H^3 i+1, j + H^3 i, j\right)}. \end{aligned} \tag{14}$$

The texture unit in this Letter is divided into 100×100 ($M = 100$, $N = 100$) nodes, and (13) is iteratively solved using the over-relaxation iterative method in [12, 20], as follows:

$$P_{i,j}^{k+1} = \omega R_{i,j} + (1 - \omega) P_{i,j}^k. \tag{15}$$

The terms $R_{i,j}$ and ω are given by

$$\begin{cases} R_{i,j} = AP_{i+1,j}^k + BP_{i-1,j}^k + CP_{i,j+1}^k + DP_{i,j-1}^k + E, \\ \omega = \dfrac{4}{2 + \sqrt{4 - \left[\cos\left(\pi/N - 1\right) + \cos\left(\pi/M - 1\right)\right]^2}}. \end{cases} \tag{16}$$

After solving the pressure of the oil film using the above method, the bearing capacity of the oil film can be calculated numerically using the compound trapezoidal formula

$$W = \int_0^{L_y} \int_0^{L_x} p\mathrm{d}x\mathrm{d}y = \frac{L_x L_y}{4MN} \sum_{i=0}^{M} \sum_{j=0}^{N} \left[T_{i,j} p(x_i, y_j) \right]. \tag{17}$$

The terms x_i and y_j are described as $(iL_x)/M$ and $(jL_y)/M$, and $T_{i,j}$ can be given as

$$T(i,j) = \begin{bmatrix} 1 & 2 & 2 & \cdots & 2 & 2 & 1 \\ 2 & 4 & 4 & \cdots & 4 & 4 & 2 \\ 2 & 4 & 4 & \cdots & 4 & 4 & 2 \\ \vdots & \vdots & \vdots & \vdots & \vdots & \vdots & \vdots \\ 2 & 4 & 4 & \cdots & 4 & 4 & 2 \\ 2 & 4 & 4 & \cdots & 4 & 4 & 2 \\ 1 & 2 & 2 & \cdots & 2 & 2 & 1 \end{bmatrix}_{(N+1)(M+1)}.$$

The solution process of friction is similar to the bearing capacity and finally, the coefficient of friction can now be found from (8).

4.3. Simulation: In the gap seal hydraulic system, the piston speed is in the range of 0.1–1 m/s. For comparison with the literature [12], other simulation parameters are given with the same working conditions in Table 1.

The solution and simulation of the oil film pressure are implemented using a MATLAB.

5. Results and discussion

5.1. Texture optimisation-shape of the textured region: In this section, different numerical results obtained for the optimal

Table 1 Initial values of simulation parameters

Simulation parameters	values
oil dynamic viscosity η, Pa s	0.04678
density of oil ρ, g/cm^3	0.897
sliding velocity of the piston U, m/s	0.75
gap between cylinder and piston h_0, μm	2
depth of texture h_p, μm	1.5
standard atmospheric pressure p_0, Pa	101325
saturated vapour pressure of hydraulic oil p_{cav}, Pa	101325
length of square control unit $L_x \times L_y$, μm	1000 × 1000

diamond-like texture are presented. To obtain optimal texture effects and the best friction performance in these configurations, the shape of the diamond will be changed through its diagonals. Since the parameters (a, b) are half of the diagonals, their values both range from zero to 0.5. Three different effects of these parameters are explained below:

(i) Fig. 7 presents the hydrodynamic lift with different values of (a, b). Clearly, texture aspect significantly influenced the texture performance. When $a = 0.5$ and $b \in (0.35, 0.4)$, the hydrodynamic lift of the oil film on the textured surface reaches a maximum (0.9226), and the dynamic pressure lubrication effect is the most effective. That is when the diamond shape is horizontally distributed, its bearing capacity is relatively large ($a > b$).

(ii) Fig. 8 presents the friction force, which changes in magnitude with the parameters (a, b). Evidently, the larger the diamond texture, the lower the friction of the textured surface.

(iii) Moreover, Fig. 9 shows the friction coefficient on the surface of the cylinder, which is determined from the bearing capacity and friction. When $a = 0.5$ and $b \in (0.35, 0.45)$, the friction between the piston and cylinder reaches a minimum (0.0283), providing the best friction performance.

In summary, the size and direction of the diamond texture on the hydraulic cylinder surface play an important role in the friction performance. The best diamond texture can be obtained with $a = 0.5$, $b = 0.4$, a diamond angle of 77.3° and texture area ratio of 0.4 (Fig. 10*a*). Then, the hydrodynamic lift is 0.9223 and the friction coefficient is 0.0283. In addition, the distribution of the film pressure is shown in Fig. 10*b*, which is consistent with the results in the literature [17].

Moreover, the textured surface can be demonstrated to have an additional capacity to support the oil film and has better frictional properties than the non-textured surface. Different textures produce different lifting force and frictional properties. The friction performance of this optimal diamond texture is nine times better than that in the literature [12] (see Fig. 11).

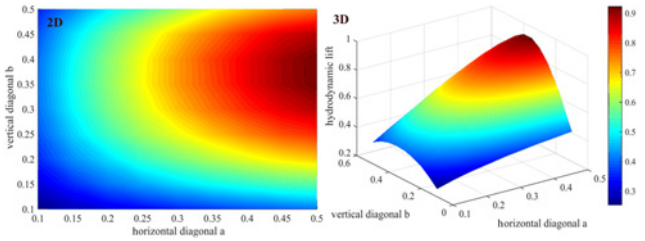

Fig. 7 *Distribution of the hydrodynamic lift on the hydraulic cylinder surface*

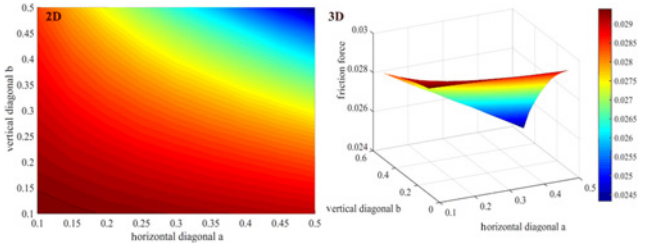

Fig. 8 *Distribution of the friction force on the hydraulic cylinder surface*

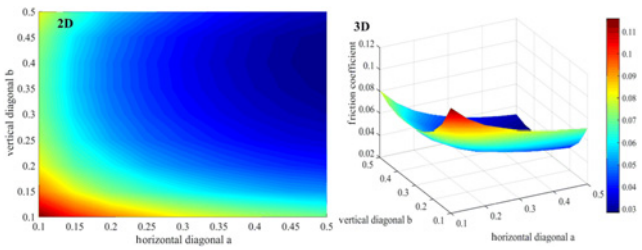

Fig. 9 *Distribution of the friction coefficient on the hydraulic cylinder surface*

5.2. Further optimisation – optimal texture depth and gap

5.2.1. Changes of texture depth (h_p): The depth of the texture is an important parameter that greatly influences the surface properties of the friction pair. Fig. 12 shows that the additional load capacity first increases and then decreases. In contrast, the friction coefficient first decreases and then increases because of the nearly constant friction. The deeper texture will enhance the additional load capacity according to (1). However, when the depth increases to a certain value, the lubricating oil begins to flow backward. With the increasing depth, the counter-current area increases and weakens the bearing capacity

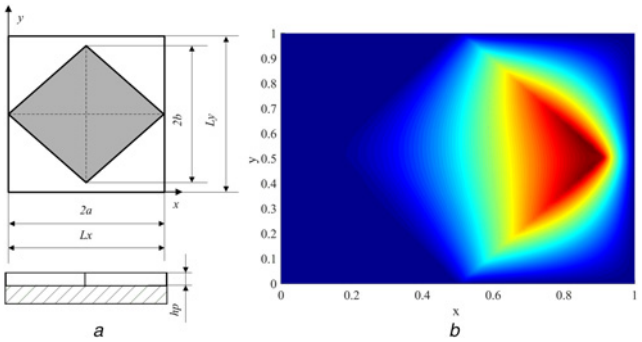

Fig. 10 *Optimal texture showing the*
a Shape
b Distribution of the film pressure

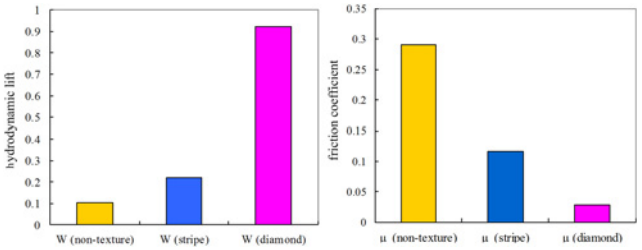

Fig. 11 *Comparison of the non-textured, striped texture and diamond textured surfaces*

doi: 10.1049/mnl.2018.0026

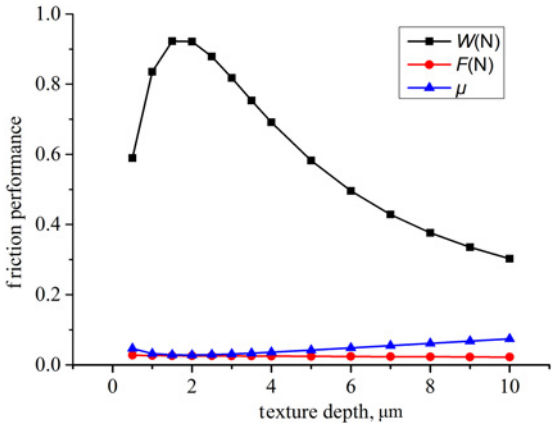

Fig. 12 *Relationship between the texture depth and friction performance*

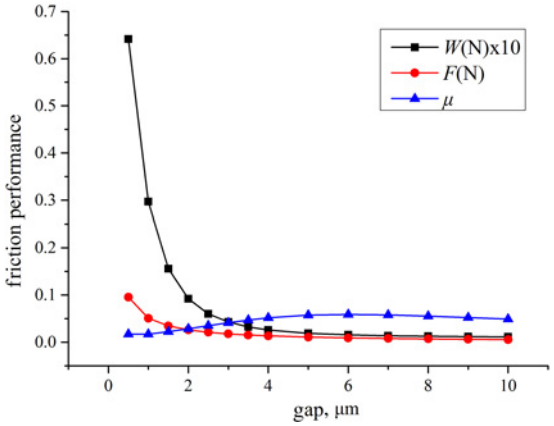

Fig. 13 *Relationship between the gap and friction performance*

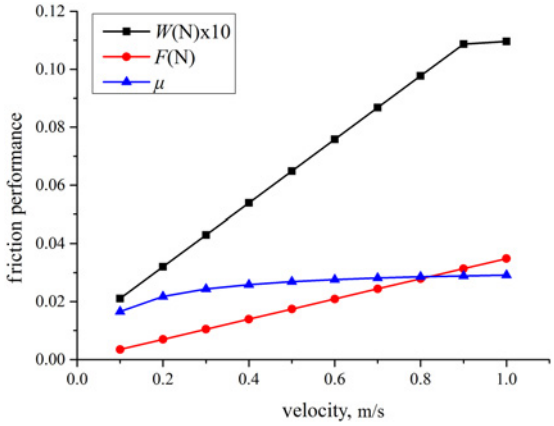

Fig. 14 *Relationship between the piston velocity of piston and friction performance*

of the texture. Therefore, the best texture depth is in the range from 1.5 to 2.

The results show that the depth of the texture mainly affects the film bearing capacity, which facilitates improving the piston eccentricity and increasing the cylinder response speed.

5.2.2. Changes of gap (h_0): In real situations, the gap between the hydraulic cylinder and the piston may vary due to machining errors, assembly errors etc. These changes will also affect the frictional properties of the textured surface (Fig. 13). An important transition node exists when the gap is equal to 2. When it is >2, the friction performance changes only slightly. In contrast, if it is <2, the bearing capacity and friction coefficient are better, which is difficult to achieve due to processing level restrictions.

For the gap-sealed hydraulic cylinder, an increase in the clearance means an increase in the amount of leakage; although the clearance increases, the friction coefficient tends to decrease slightly.

5.3. Impact of speed (U): The influence of the piston velocity on the friction coefficient is small because as the velocity increases, the bearing capacity and friction force also increase (Fig. 14). This result is beneficial for accelerating and decelerating the piston.

6. Conclusions: By simulating and optimising the rhombic texture of shark skin on the inner surface of the cylinder, the best texture shape is determined. This optimised texture exhibits better friction performance for the gap seal hydraulic cylinder that the striped texture. At the same time, considering the influence of the texture parameters, the depth of texture and cylinder gap is also optimised, which further improves the friction performance of the cylinder surface.

The main conclusions of this work are summarised below.

(i) The diamond-like textured surface of the cylinder has an additional capacity to maintain the oil film and has better frictional properties than the non-textured surface. Different diamond-like textures produce a different lifting force and frictional properties.

(ii) The rhombic texture imitating shark skin has superior properties to those of the striped texture. Under the same working conditions, the lift of the diamond texture is nine times higher than that of the striped texture, while the friction coefficient of the surface is one-quarter of that of the striped texture, which will greatly improve the hydraulic cylinder friction properties and responsiveness.

(iii) The depth of the texture and cylinder clearance significantly affected the performance of the friction pair. An optimal depth and gap of 1.5 and 2, respectively, provide the best friction performance. These values help solve the problem of improving the leakage of the gap seal cylinder. In addition, the piston speed has little effect on the friction performance.

This work can guide hydraulic cylinder systems towards greatly improved friction and responsiveness.

7. Acknowledgments: The authors are grateful for financial support from the Natural Science Foundation of China (research on the technology of controlled-variable clearance and lubricating mechanism of sealing surface bionic texture about high speed hydraulic cylinders), grant no. 51475338 and (study on elastohydrodynamic lubrication mechanism and structural optimisation of heterogeneous friction interface of the heavy-load and high-speed clearance gap seal hydraulic servo cylinders), grant no. 51705377.

8 References

[1] Tomanik E.: 'Modeling the hydrodynamic support of cylinder bore and piston rings with laser textured surfaces', *Tribol. Int.*, 2013, **59**, pp. 90–96

[2] Profito F.J., Vladescu S.-C., Rhoff T., *ET AL.*: 'Transient experimental and modeling studies of laser-textured micro grooved surfaces with a focus on piston-ring cylinder liner contacts', *Tribol. Int.*, 2017, **113**, pp. 125–136

[3] Rao T.V.V.L.N., Abdul-Rani A.-M., Nagarajan T., *ET AL.*: 'Analysis of slider and journal bearing using partially textured slip surface', *Tribol. Int.*, 2012, **56**, pp. 121–128

[4] Gropper D., Wang L., Harvey T.: 'Hydrodynamic lubrication of textured surfaces: a review of modeling techniques and key findings', *Tribol. Int.*, 2016, **94**, pp. 509–529
[5] Sharma V, Pandey P.M.: 'Recent advances in turning with textured cutting tools: a review', *J. Clean. Prod.*, 2016, **137**, pp. 701–715
[6] Sugihara T., Enomoto T.: 'Performance of cutting tools with dimple textured surfaces: a comparative study of different texture patterns', *Prec. Eng.*, 2017, **49**, pp. 52–60
[7] Meng X., Bai S., Peng X.: 'Lubrication film flow control by oriented dimples for liquid lubricated mechanical seals', *Tribol. Int.*, 2014, **77**, pp. 132–141
[8] Guo F., Jia X., Wang L., *ET AL.*: 'The effect of axial position of contact zone on the performance of radial lip seals with a texturing shaft surface', *Tribol. Int.*, 2016, **97**, pp. 499–508
[9] Zhan C., Deng J., Chen K.: 'Research on low-friction and high-response hydraulic cylinder with variable clearance', *J. Mech. Eng.*, 2015, **51**, (24), pp. 161–167
[10] Liu Y., Li G.: 'A new method for producing 'lotus effect' on a biomimetic shark skin', *J. Colloid Interface Sci.*, 2012, **388**, pp. 235–242
[11] Lu Y., Liu Z.: 'Lubrication performance of the grid-patterned microcirculation surface', *Tribology*, 2013, **33**, (4), pp. 357–362
[12] Yu G., Zeng L., Lu Y.: 'Numerical analysis of the friction property of microgroove texture on the piston surface of hydraulic cylinder', *J Wuhan Univ. Sci. Technol.*, 2015, **38**, (6), pp. 436–439
[13] Gachot C., Rosenkranz A., Hsu S., *ET AL.*: 'A critical assessment of surface texturing for friction and wear improvement', *Wear*, 2017, **372–373**, pp. 21–41
[14] Mao Y., Zeng L., Lu Y.: 'Modeling and optimization of cavitation on a textured cylinder surface coupled with the wedge effect', *Tribol. Int.*, 2016, **104**, pp. 212–224
[15] Wen S., Huang P.: 'Principles of tribology' (Tsinghua University Press, Beijing, 2012, 4th edn.)
[16] Etsion I.: 'Modeling of surface texturing in hydrodynamic lubrication', *Friction*, 2013, **1**, (3), pp. 195–209
[17] Dobrica M.B., Fillon M., Pascovici M.D., *ET AL.*: 'Optimizing surface texture for hydrodynamic lubricated contacts using a mass-conserving numerical approach', *J Eng. Tribol.*, 2014, **224**, pp. 737–750
[18] Woloszynski T., Podsiadlo P., Stachowiak G.W.: 'Evaluation of discretisation and integration methods for the analysis of hydrodynamic bearings with and without surface texturing', *Tribol. Lett.*, 2013, **51**, pp. 25–47
[19] Pei S., Ma S., Xu H, *ET AL.*: 'A multiscale method of modeling surface texture in hydrodynamic regime', *Tribol. Int.*, 2011, **44**, pp. 1810–1818
[20] Golub G.H., Varga R.S.: 'Chebyshev semi-iterative methods, successive over-relaxation iterative methods, and second order Richardson iterative methods', *Numer. Math.*, 1961, **3**, pp. 147–156

doi: 10.1049/mnl.2018.0026